Large eddy simulation of transitional separated flow over a low Reynolds number cambered airfoil

Alison Zilstra
Department of Mechanical Engineering
University of Waterloo
Waterloo N2L 3G1, Canada
Email: alison.zilstra@uwaterloo.ca

David A. Johnson
Department of Mechanical Engineering
University of Waterloo
Waterloo N2L 3G1, Canada

ABSTRACT

The accurate simulation of the aerodynamic behaviour of low Reynolds number (Re) cambered airfoils requires the ability to capture the transitional separated boundary layer (BL) that occurs naturally on the surface of the airfoil. In this study, simulations are performed using a modern cambered airfoil designed for use in low Re applications, which are an advancement from previous studies using flat plate geometries or symmetric NACA airfoils. The cambered SD 7037 airfoil is simulated using wall-resolved large eddy simulation (LES) at a modest Re of 4.1×10^4 *and at* 1°*,* 5°*, and* 7° *angles of attack (AOAs), with results validated against experimental data. Simulated predictions of pressure and skin friction coefficients clearly capture the correct location of the laminar separated bubble (LSB) which forms during the natural BL transition process. Sensitivity to elevated inflow turbulence is found to cause early BL reattachment at higher AOAs without impacting the location of BL separation. An integral BL analysis verifies the accuracy of the simulated velocity profiles against experimental values. The scale of horseshoe structures visualized*

in the transitional BL is larger in comparison to airfoil chord length than what is seen in previous simulations at Re on the order of 10^5, which highlights the importance of investigating cambered airfoils at a modest Re.

NOMENCLATURE

c airfoil chord, m

C_f skin friction coefficient

C_p pressure coefficient

Re Reynolds number

h LSB height, m

H shape factor

α angle of attack, deg

δ^* displacement thickness, m

θ momentum thickness, m

INTRODUCTION

Transitional separated flow over low Reynolds number (Re) airfoils is unavoidable in certain applications and can alter the expected aerodynamic performance of the airfoil. Modern airfoils specifically designed for operation at a low Re, defined here as a chord based Re of less than 5×10^5, are most commonly cambered airfoils and are used in applications such as small wind turbines (SWT), turbomachinery, micro air vehicles (MAV) and unmanned air vehicles (UAV). These applications can operate at modest Re, often Re $< 1 \times 10^5$, which is a lower Re than has been typically investigated for transitional separated flow in the past.

Transitional separated flow occurs when the natural boundary layer (BL) transition is disrupted by a laminar separation bubble (LSB). The LSB forms when the airfoil curvature and associated pressure gradient causes BL separation, which is followed by BL transition and reattachment [1, 2]. Due to the unforced nature of this process, any simulation method must sufficiently capture the small-scale and unsteady behaviour that drives the natural BL transition [3], as well as the

instability in the separated shear layer that leads to the formation of the LSB [4].

Transitional separated flow has been successfully simulated using direct numerical simulation (DNS) [5–10] and large eddy simulation (LES) [2, 11–19] to capture this sensitive BL behaviour. Studies have also used Reynolds-averaged Navier-Stokes (RANS) to predict LSB formation on airfoils using the $\gamma - \mathrm{Re}_{\theta t}$ model [20, 21], however this method is unable to provide the transient information required for determining detailed airfoil performance. LES is an accessible alternative to the computationally expensive DNS method while also providing detailed transient data, and therefore is preferable for aerodynamic design purposes.

The validation of both DNS and LES simulations are extremely limited by the availability of detailed quantitative experimental data, especially for airfoils at modest Re of less than 1×10^5. For this reason, prior efforts in DNS and LES simulation of this type of flow have been focused on flat plate geometries as well as airfoils not commonly used in the mentioned low Re applications, such as symmetric NACA profiles. Additionally, airfoils operating at modest Re often have an elongated LSB in comparison with higher Re cases, with the LSB covering as much as 50% of the airfoil chord (c). It is important to validate the simulation of an elongated LSB on a cambered low Re airfoil to ensure that current methods are capable of predicting the BL transition and separation and reattachment locations.

This work is a numerical study of the aerodynamic performance of the SD 7037 cambered low Re airfoil, which is specifically designed for use in low Re applications and is known to experience transitional separated flow at modest Re. Wall-resolved LES is applied to investigate the airfoil performance at $\mathrm{Re} = 4.1 \times 10^4$ and at 1°, 5°, and 7° angles of attack (AOA) which provides a range of different LSB lengths and locations. Recent experiments by Ghorbanishohrat [22] proved the existence of a LSB on the SD 7037 airfoil for a range of modest Re, and also employs a method to determine skin friction coefficients to pinpoint the separation and reattachment locations for the LSB. This experimental data will be used to validate the LES results using multiple methods of comparison which cover different aspects of the BL to provide high quality validation of the LES prediction of transitional separated flow over a low Re cambered airfoil.

Low Re Boundary Layer Transition

Analyzing the natural BL transition process for a low Re cambered airfoil requires capturing the small scale transient behaviours at different stages of transition, as well as predicting the formation of a LSB. Fig. 1 illustrates the flow dynamics of a cambered airfoil with a LSB forming while the BL transitions. Within the transition region, the natural BL transition behaviours develop in a similar manner to the classic flat plate BL transition described by Schlichting [3], until interrupted by laminar separation.

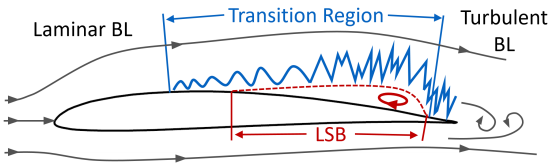

Fig. 1. Idealized transitional separated boundary layer over a low Re cambered airfoil, dashed lines for LSB and solid lines for transition region

Laminar separation will occur after the location of minimum pressure, known as the suction peak, where the BL experiences an adverse pressure gradient due to the curvature of the airfoil. This adverse pressure gradient reduces the stability of the BL [3], and at the point of separation, the adverse pressure gradient has become sufficiently strong to overcome the low momentum of the laminar or transitioning BL [16]. Once the BL is separated, the remaining transition to turbulence is triggered by a Kelvin-Helmholtz (K-H) instability in the shear layer [2], which develops due to the difference between the velocity in the separated BL and the reverse flow that is present within the LSB [6]. The amplification of the K-H instability results in the formation of spanwise vortices (also called K-H rolls [13]), which enhances near-wall momentum exchange and increases mixing between the layers, leading to reattachment of the BL to form the LSB [5, 6]. In some cases, such as when laminar separation occurs closer to the trailing edge (TE) of the airfoil [22] or the airfoil is approaching stall [16], the BL is unable to reattach and therefore has a laminar separated BL rather than a fully formed LSB.

DNS and LES of Low Re Transition

Numerous computational studies have been conducted on low Re transitional separated flow over the past 20 years. A common method to simplify the geometry uses an experimental method of a flat plate in a wind tunnel with a curved upper wall to impose the necessary pressure gradient on the surface. Using a flat plate removes the complexities of airfoil curvature by artificially adding the associated pressure behaviour, which allows control over the formation of the LSB and provides a large downstream region to allow a fully developed reattached turbulent BL to develop. This has been successfully investigated with both DNS [5, 6] and LES [11–13]. The DNS study by Brinkerhoff and Yaras [6] is a good example of the detailed analysis possible when using the extended streamwise length of a flat plate (in comparison to an airfoil). At Re $= 3.26 \times 10^5$, the authors show the visualization of the roll up of the separated shear layer and subsequent formation of large scale turbulent wave-packets after reattachment. Roberts and Yaras [12] conducted LES simulations on a coarse DNS mesh which reproduced LSB velocity profiles within 15% of experimental data, which they considered good agreement. More recent LES work by Li and Yang [13] examined a flat plate with an elliptical leading edge (LE), which adds complexity when compared to the other mentioned simulations with a slip wall preceding the flat plate and no LE. At Re $= 8.4 \times 10^4$ they showed the ability of LES to replicate experimental results while requiring a lesser computational expense than a DNS simulation.

However, experimental particle image velocimetry (PIV) results by Burgmann *et al.* [23] call into question the accuracy of this flat plate method through examination of a cambered SD 7003 airfoil at the modest Re of 2×10^4. The authors found that the change in pressure gradient resulting from different experimental AOAs had a different effect on the LSB characteristics when compared to other studies which altered the pressure gradient over a flat plate.

Simulations that incorporate more complex geometry into the simulation of transitional separated flow are those using symmetric NACA airfoil profiles. These profiles are commonly chosen due to the well established behaviour of these airfoils through past experimental work, and new simulations fill the gaps in knowledge for the transitional separated flow that can occur at low Re. These profiles have been studied using DNS [7–10, 14] and LES [14–16], and the geome-

try represents the airfoil curvature without concerns about the accuracy of an imposed pressure gradient [23]. The recent work by Smith and Ventikos [14] compares DNS and LES over a NACA 0012 airfoil at Re $= 1 \times 10^5$ and 4° AOA to assess the impact of LES modeling techniques on the accuracy of the prediction. Ziade *et al.* [16] use LES and PIV to investigate laminar separation and transition on a NACA 0025 airfoil at Re $= 1 \times 10^5$ and $5^\circ, 12^\circ$ AOA.

The Re range for the mentioned NACA studies is generally between 1×10^5 and 5×10^5 or at a high AOA, which places the LSB close to the LE of the airfoil and results in a turbulent BL for the majority of the airfoil surface. For example, Thomareis and Papadakis [7] performed DNS studies on the NACA 0012 airfoil at a more modest Re of 5×10^4 and 5° AOA, where a LSB formed from $x/c = 0.2$ to 0.6. When compared to Smith and Ventikos, with a LSB from $x/c = 0.4$ to 0.6, it is clear that the lower Re causes an elongated LSB. However, in both cases the reattachment is well before the TE and Smith and Ventikos note their findings would not necessarily apply to cases where the BL is transitional at the TE of the airfoil [14]. These studies therefore do not attempt simulation of the interaction of the transitional BL with the TE, which is especially complex when the separated shear layer does not reattach and interacts with the flow from the pressure side. This specific situation is examined in the 1° AOA case covered in this paper.

An application of interest that falls on the lower end of the Re range is low Re turbomachinery cascades, such as the DNS of a T106a cascade [5] and LES of a V103 compressor cascade [11]. Lardeau *et al.* [11] highlights the complexities that arise in the relatively modest Re experienced by low pressure cascades, in their case Re $= 1.4 \times 10^5$, and the sensitivity of the separation bubble dynamics to the geometric, inflow, and boundary conditions of the simulation. While pressure cascades often have elongated LSBs that can be located near the TE, the geometry of airfoils specifically designed for SWTs, MAVs and UAVs are generally cambered airfoils with a larger thickness than found in compressor cascades.

Another significant difference between compressor cascades and the cambered airfoil applications is the boundary conditions required for the simulations. There is a periodicity that occurs in the wall-normal direction due to the adjacent blades on the cascade, which constrains the flow surrounding the airfoil in a way not seen in the external flow conditions of a low Re cambered airfoil

application. The channeling of the flow between two blades on the cascade will have an impact on the BL transition and is likely to result in different aerodynamic behaviour. A computational benefit is also present in the cascade, since the periodic constraint of the adjacent blade can greatly reduce the size of the required computational domain, decreasing the computational cost and time required when compared to an external flow cambered airfoil.

LES simulations of cambered airfoils at appropriately modest Re have been previously completed using the SD 7003 airfoil [2, 17, 18] and an airfoil profile from a wind turbine blade [19]. These works have been completed for the Re range of 10^4 to 10^5 and at 4° AOA, with the exception of Galbraith and Visbal [17] which covers an AOA range from 2° to 14°. Breuer [18] and Lobo *et al.* [19] investigated the impact of inflow turbulence on the formation of the LSB, confirming that an increase in turbulence intensity causes the LSB length to decrease and eventually vanish. However, as with the other low Re airfoil simulations, the availability of experimental validation data on these less commonly investigated airfoils is limited and therefore prevents the complete validation of the LES simulation of the transitional separated BL behaviour.

NUMERICAL METHOD

The wall-resolved LES simulations were performed using the commercial software ANSYS Fluent, Release 20.2 to analyze the transient behaviour of a transitional separated BL over a low Re cambered airfoil. The chosen subgrid scale (SGS) model is the dynamic Smagorinsky-Lilly model, as it has been shown that a dynamic model is better able to capture low Re BL behaviour [14]. The mass and momentum conservation equations were solved in the incompressible form to resolve the BL transition behaviour and LSB location [6].

The flow was initialized with the Transition Shear Stress Transport (SST) $k-\omega$ RANS model (also known as $\gamma-\mathrm{Re}_{\theta t}$) to improve LES convergence time. After numerous test cases, simulations were run at a time step of $\Delta t = 4 \times 10^{-6} s$ for 3 domain-based mean flow residence times (MFRT), where only data from the final 2 MFRT was processed (1 domain-based MFRT is equivalent to 24 chord-based MFRT). Convergence criteria were set at 5×10^{-5} for all parameters. The SIMPLEC pressure-velocity coupling scheme was used, with bounded CDS as the discretization scheme

and bounded second order implicit as the transient formulation. To decrease computing time, simulations were run using a high performance computer cluster in the Digital Research Alliance of Canada network [24].

Case Geometry

Previous work by the authors' research group experimentally examined the transitional BL present on the SD 7037 airfoil [22,25], which was specifically designed for low Re applications [26]. Experiments consisted of a 2D cambered airfoil with a constant chord of 25.8 mm and span of 152.4 mm in a closed loop wind tunnel (152.4 mm square cross-section). The LES simulation is set up to replicate these flow conditions and geometry, including a rounded TE of r = 0.045 mm to match the manufactured airfoil. Velocity measurements of the flow around the airfoil using PIV was conducted by Ghorbanishohrat [22], specifically focusing on the boundary layer transition process, which serves as the validation for the simulated flow parameters. From the experimental study, a Re of 4.1×10^4 and static AOAs of 1°, 5°, and 7° were selected for the LES simulations. The main geometry and numerical details are summarized in Table 1.

Table 1. Geometry and numerical details

Airfoil Profile		SD 7037
Angle of Attack	α	1°, 5°, 7°
Chord	c	0.0258 m
Span	b	0.2c
Inflow Velocity	U_∞	23.84 m/s
Reynolds Number	Re	4.1×10^4
Time Step	Δt	4×10^{-6} s

Meshing and Boundary Conditions

The domain is a C-mesh with 12 chord length boundary offsets (0.31 m), and a span of 0.005 m, or 0.2c, as shown in Fig. 2. The $12c$ boundary offsets are consistent with classic C-mesh

geometry, and the spanwise extent is consistent with the $0.2c$ commonly seen in simulations of transitional flow over symmetric NACA airfoils [7, 14] and cambered airfoils [17–19]. The boundary conditions are as shown in Fig. 2, with the airfoil surface as a no-slip wall, the curved and horizontal surfaces as velocity inlets, the spanwise boundary condition as periodic, and vertical outflow surface as a pressure outlet.

A known issue with LES is the difficulty of generating an accurate replication of inflow turbulence conditions, since the model can be quite dissipative [27]. Accurate turbulence generation is necessary for transitional separated flow since increasing turbulence has been shown to cause a decrease in the bubble length [5, 11, 18, 19]. Synthetic turbulence generation methods are generally favoured for practical applications [28], and are included in commercial computational fluid dynamics software packages. Roberts and Yaras [12] used a synthetic method built-in to ANSYS CFX to generate turbulence for the simulation of transitional separated flow on a flat plate. For this work, the ANSYS Fluent built-in Spectral Synthesizer method was chosen and the inflow turbulence was introduced in a $4.75c$ segment of the curved inlet, located directly upstream of the airfoil. This method generated the desired level of inflow turbulence at the airfoil, while keeping the computational cost low by reducing the complexity of the calculations in the farfield of the domain. The turbulent intensity at the inlet is artificially increased to account for the dissipation that occurs between the inlet and the airfoil [11], which results in a turbulent intensity of 1% at a location 24 mm upstream of the LE as measured experimentally [22, 29]. Tests of the inlet turbulence dissipation determined the ideal parameters to be a specified inlet turbulent intensity of 4.4% and length scale of 11 mm.

The mesh consists of 2.6 million elements with 300 chordwise and 50 spanwise divisions (Fig. 3) and the y^+ is less than 0.5 at the airfoil surface for all simulated AOAs, with the average y^+ ranging from 0.21 for 1° AOA to 0.27 for 7° AOA. Pope [30] suggests that accurate wall-resolved LES requires 80% of the turbulent kinetic energy to be resolved (i.e. not calculated through SGS modelling). To achieve this in the BL, Pope recommends that the subgrid filter length Δ (equal here to the cubed root of the cell volume [31]) is on the order of the viscous length scale, δ_v, for

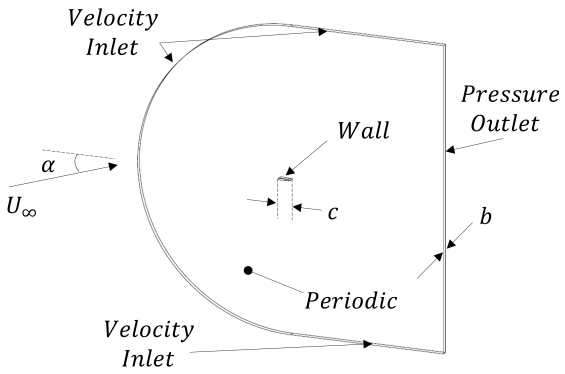

Fig. 2. Schematic of computational domain

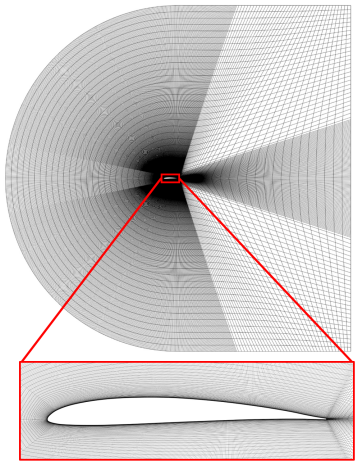

Fig. 3. C-Mesh with close up view of mesh quality around airfoil

$y^+ < 20$. Viscous lengthscale is defined as

$$\delta_v \equiv \nu \sqrt{\frac{\rho}{\tau_w}} \tag{1}$$

and is therefore dependent on the local shear stress in the BL for each AOA simulated. After examining the 1° and 7° AOA cases, the BL was found to meet this condition with $\Delta \leq 10\delta_v$ for the suction side BL and with an average of $2.4\delta_v$ at the surface and $4.5\delta_v$ at $y^+ = 20$.

RESULTS

Flow Structure Visualization

A useful method of visualizing the coherent flow structures within the BL transition is through iso-surfaces of Q-Criterion, defined as the second invariant of the velocity gradient [32]. Fig. 4 shows the Q-criterion iso-surface at a value of $5 \times 10^7\ s^{-2}$ for the final time step of each simulated AOA. Flow is from the lower left to the top right, showing the suction side of the airfoil and can be compared with the transition process outlined in Fig. 1. The Q-criterion is coloured with the velocity magnitude, $|V|$, non-dimensionalized with the inflow velocity, U_∞, to better visualize the height and shape of the structures formed over the LSB and after BL reattachment. The locations

of BL separation and reattachment are indicated by the white dashed lines, where applicable, and exact x/c values for these locations, found in Table 2, were determined using the skin friction coefficient results presented later in this paper.

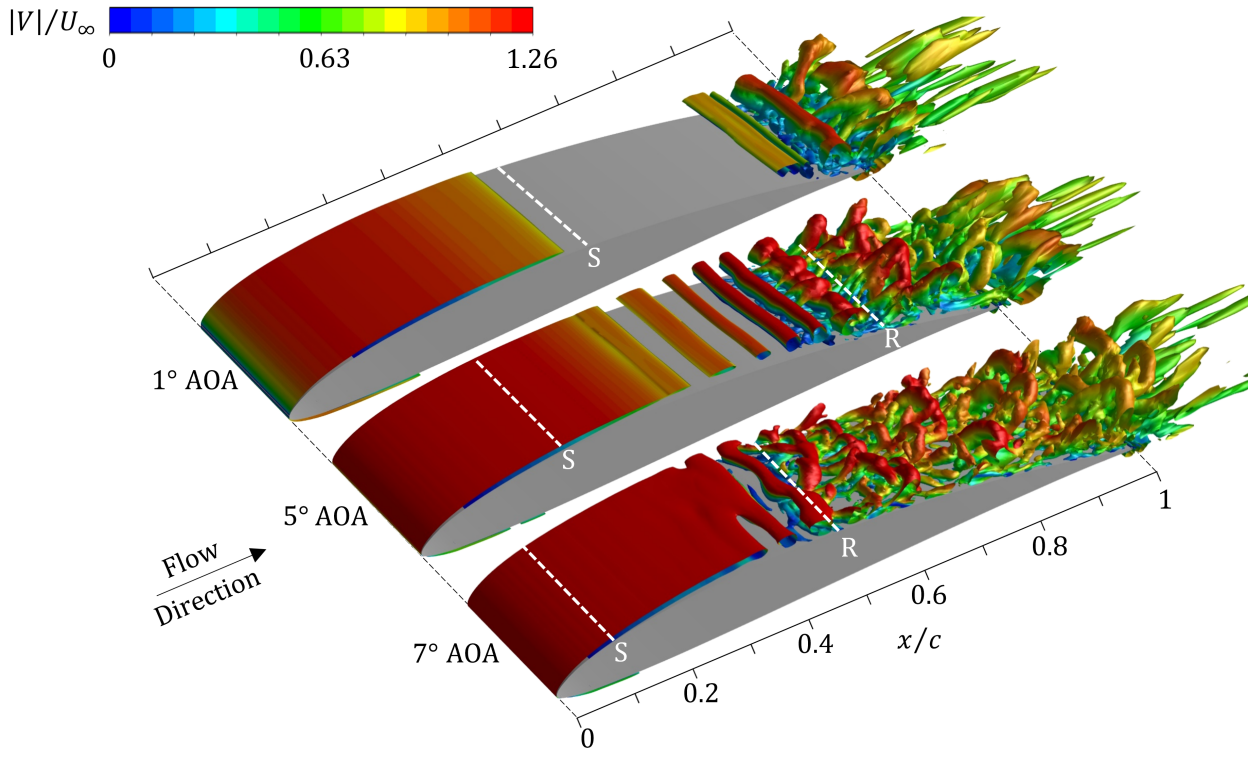

Fig. 4. Q-Criterion iso-surface of $5 \times 10^7\ s^{-2}$ for $1°$, $5°$ and $7°$ AOAs, coloured by non-dimensional velocity magnitude. White dashed lines indicate location of BL separation (S) and reattachment (R), where applicable

For $1°$ AOA, laminar separation is approximately seen at the abrupt stop of the Q-Criterion iso-surface which forms from the LE of the airfoil. At the TE, the transitional BL remains largely two-dimensional (2D) and due to insufficient growth of K-H instabilities it does not progress into the portion of the transition process where significant spanwise patterns are formed. The development of increasingly complex spanwise structures occurs after BL reattachment, as seen the $5°$ and $7°$ AOA results. The elongated LSB and accompanying slower transition to turbulence in the $5°$ AOA case shows the growth of the 2D K-H rolls that are initiated by the K-H instability [13], and the formation of horseshoe vortices after reattachment [3]. The horseshoe vortices have elongated legs extending down to the airfoil surface with the heads of the horseshoes aligning with the K-H

rolls that developed in the separated shear layer. These waves of horseshoe vortices developing in the reattached BL are a similar scale to the cambered airfoil simulations at $Re = 6 \times 10^4$ by Galbraith and Visbal [17] and Breuer [18], the symmetric NACA airfoil simulation at $Re = 5 \times 10^4$ by Thomareis and Papadakis [7], and the flat plate results of Brinkerhoff and Yaras [6]. In airfoil simulations at a higher Re [11, 14, 16, 19], the scale of the horseshoe structures in the reattached BL is smaller in comparison to the airfoil chord, K-H roll size and LSB length. This trend can be clearly seen in a comparison of the symmetric NACA airfoil simulation by Thomareis and Papadakis [7] and the works of Smith and Ventikos [14] and Ziade *et al.* [16] at a similar AOA and double the Re.

Table 2. Boundary layer separation, transition and reattachment locations, $Re = 4.1 \times 10^4$

Angle of Attack	x/c Location		
	Separation	Transition	Reattachment
1°	0.54	0.88	- -
5°	0.30	0.65	0.84
7°	0.13	0.40	0.54

The 7° AOA BL transition contains similar structures as the 5° AOA result, however it is visibly much more disorganized with increasing x/c. This indicates an accelerated transition to turbulence, which is expected due to the shortened LSB as well as the higher pressure and velocity gradients. The 7° AOA results are similar to those seen in previous simulations of transitional separated flow [14,16], which use symmetric NACA airfoils at a higher Re on the order of 10^5 and 4° or 5° AOAs. In these higher Re cases, the BL transition occurs earlier and the transitional separated BL process is condensed into a shorter chordwise distance. Due to the accelerated transition in those studies, any remnant of the K-H spanwise rolls disappears at reattachment, meaning that the horseshoe vortices and other complex structures are no longer in spanwise alignment. The mentioned differences in LSB length and the scale of the horseshoe vortices in the attached BL clearly show the importance of numerically investigating the transitional separated BL at increas-

ingly modest Re, since the sensitive transition process includes larger structures that will have a greater impact on airfoil performance.

Pressure Distribution

The time averaged pressure coefficient (C_p) results are shown for the suction side of the airfoil in Fig. 5, compared against the experimental results [22]. The simulated C_p has a consistently higher magnitude than the experimental results, and this is most notable at the suction peak (minimum C_p). A unique aspect of the experiments by Ghorbanishohrat [22] is that surface pressure measurements were determined through integration of the PIV velocity measurements in the BL. This method of pressure determination was necessary since the small scale of the airfoil prevented the usage of static pressure taps. While the reported statistical uncertainty for averaged velocity components was 0.42%, the accuracy of this method of calculating C_p is limited by the PIV resolution close to the wall, and introduces more error closer to the LE of the airfoil where the BL is thin. It is therefore expected that the experimental suction peak measurements will be of lower magnitude than the simulated values, which is the case for the presented results. This is also expected to be the reason for the greater magnitude of the C_p values generated by the LES simulation, placing more emphasis on the agreement of the changes in C_p gradient with respect to x/c for validating the pressure behaviour at the airfoil surface. Additional analysis comparing the PIV resolution to the near-wall resolution of the LES simulation can be found in the *BL Separation and Reattachment* section of this paper.

A C_p plot with a fully formed LSB will feature the indicative transition ramp [33], which begins with the levelling off of the C_p curve at the location of laminar separation (labelled S in Fig. 5) followed by a sharp pressure recovery at reattachment (labelled R in Fig. 5). Exact x/c locations of BL separation and reattachment can be found in Table 2. In the 1° AOA result in Fig. 5(a), the decreasing gradient indicating laminar separation can be seen at approximately $x/c = 0.55$, and there is no pressure recovery since the BL does not reattach to form the LSB at this AOA [22]. The transition ramp in the C_p curve for the 5° and 7° AOA simulations can be more clearly seen in Fig. 5(b) and 5(c), since they both have a fully formed LSB. For both AOAs, the location of separation can be seen to be in agreement with the experimental findings due to the parallel C_p curves at the

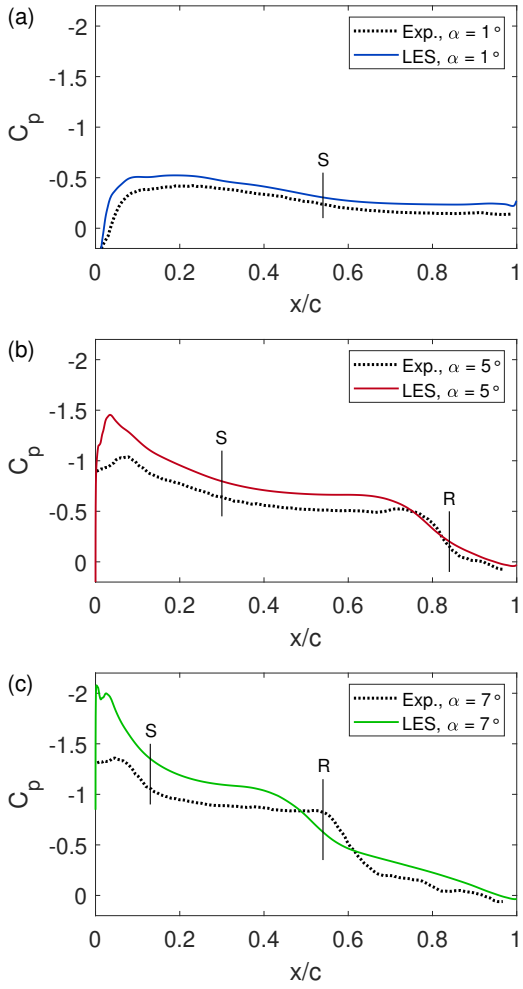

Fig. 5. Suction side C_p for (a) 1° AOA (b) 5° AOA and (c) 7° AOA compared with experimental measurements [22]. Locations of BL separation and reattachment are marked with S and R, respectively

initiation of the transition ramp. This occurs at approximately $x/c = 0.3$ for 5° AOA and $x/c = 0.13$ for 7° AOA. However, the pressure recovery occurs earlier in the LES results, showing that the BL reattaches earlier than it was found to in experiments. This can be seen when the LES and experimental results intersect at around $x/c = 0.8$ for 5° AOA and $x/c = 0.6$ for 7° AOA. Deviation of the reattachment location is more likely to occur since the separated BL is more sensitive to the free stream turbulence and higher turbulence will lead to earlier BL reattachment [5, 11, 18, 19]. This indicates that the inlet turbulence model used in the LES simulations likely generated free

stream turbulence that was slightly elevated in comparison to the experimental conditions.

Similar transition ramps have been simulated previously for cambered airfoils [2, 17–19] and NACA airfoils [7, 8, 14], though the C_p results in those cases are either unvalidated or validated against DNS results rather than experimental data. This removes the complexity of replicating the experimental free stream turbulence conditions. Ziade *et al.* [16] validated the LES generated C_p against experimental surface pressure measurements, generating an accurate C_p curve with the exception of a delay in the location of BL reattachment. This was attributed to the laminar free stream conditions (i.e. no prescribed inlet turbulence) used in the LES simulation in comparison with experimental results which were collected with an inflow turbulence intensity of 0.08%. In the presented work, the LES turbulence intensity is in agreement with the measured experimental turbulence intensity of 1% at a location 24 mm upstream of the LE [29] and therefore resulted in a more accurate prediction of the location of pressure recovery in the C_p curve. It is clear from the presented results and those of Ziade *et al.* [16] that minor differences in inflow turbulence, while not affecting the laminar separation location, can have a significant impact on the reattachment location. This further highlights the importance of high resolution experimental validation data and accurate inflow turbulence replication in LES simulations of transitional separated flow.

Boundary Layer Integral Analysis

A fundamental aspect of BL analysis is the accurate determination of integral BL variables which describe the velocity distribution within the BL and can confirm the locations of key behaviours in the transitional separated BL. Displacement thickness (δ^*) is defined as,

$$\delta^* = \int_0^\delta \left(1 - \frac{U}{U_e}\right) dy \tag{2}$$

where U_e is the edge velocity and the y-direction is perpendicular to the airfoil surface [3]. The variation in δ^* along the chord is useful for identifying the location of laminar separation since the added distance between the separated shear layer and the airfoil surface causes a noticeable increase in the measured δ^* [34].

The simulated δ^*/c for each AOA is shown in Fig. 6 with comparisons against the experimental measurements of Ghorbanishohrat [22]. The LES mean velocity profiles used to calculate δ^* were collected at a spacing of $x/c = 0.025$ (0.645 mm) in planes perpendicular to the airfoil surface. As was seen in the C_p data, the simulated magnitude of δ^*/c is larger than what was measured experimentally but the gradient of δ^*/c with x/c is in agreement. The early transition of the 7° AOA separated BL can also be seen in this data, where the simulated peak at approximately $x/c = 0.4$ occurs before the experimental peak at approximately $x/c = 0.5$.

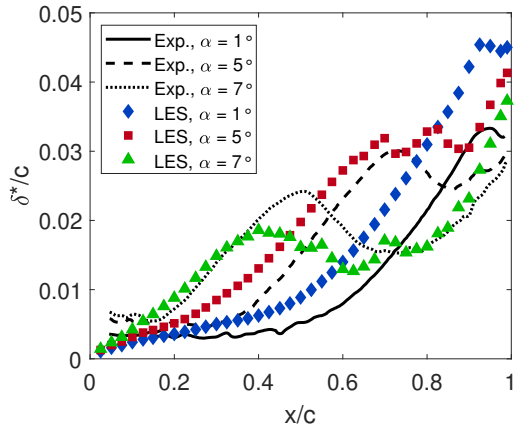

Fig. 6. Non-dimensional displacement thickness, δ^*/c vs. x/c for $\alpha = 1^\circ, 5^\circ, 7^\circ$, compared against experimental data [22]

Momentum thickness (θ) is defined as,

$$\theta = \int_0^\delta \frac{U}{U_e}\left(1 - \frac{U}{U_e}\right) dy \tag{3}$$

The θ is unaffected by laminar separation due to the negligible momentum of the fluid trapped within the bubble, however it has a significant increase in magnitude when the separated BL transitions to a high momentum turbulent BL [34, 35]. The simulated θ/c results in Fig. 7 very clearly show this abrupt increase in boundary layer momentum. This location coincides with the x/c location of the initiation of the pressure recovery of the transition ramp in the C_p results,

which is another indication of the location of BL transition. All results are in agreement with the experimental data, with minor differences in the θ/c gradients for the 5° and 7° AOA after BL transition. An interesting feature of the 7° AOA θ/c is the increase and then brief plateau that occurs twice between $x/c = 0.5$ and 0.8. This could be due to complex flow structures (such as the horseshoe vortices visualized in Fig. 4) developing at a consistent location with time and these jumps in BL momentum are likely the reason for the predicted early BL reattachment at this AOA.

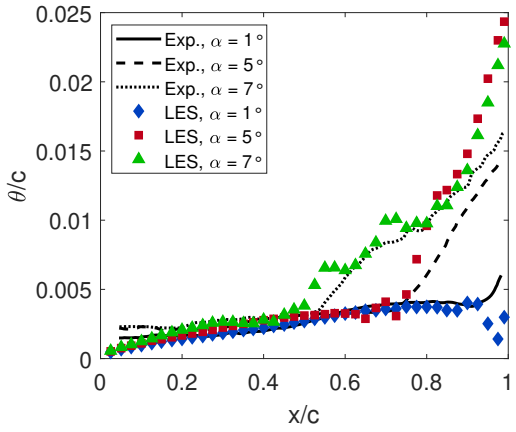

Fig. 7. Non-dimensional momentum thickness, θ/c vs. x/c for $\alpha = 1^\circ, 5^\circ, 7^\circ$, compared against experimental data [22]

A notable difference in the δ^*/c and θ/c trend occurs when $x/c \leq 0.2$, where the gradient of the experimental data is approximately zero and the simulated data has a gradient consistent with the data when $x/c > 0.2$. This shows the impact of near-wall PIV resolution on the experimental results, since the thin laminar BL near the LE is more accurately captured by the finer resolution used in the LES simulation.

While δ^* and θ are individually useful for BL analysis, when combined together in a dimensionless group they can be used to characterize the velocity profile of the BL [3]. Shape factor, H, is defined as

$$H = \frac{\delta^*}{\theta} \tag{4}$$

When using H to analyze a transitional separated BL, a clearly defined peak develops due to the delay in the increase of θ in relation to δ^*. This is seen in the simulated results in Fig. 8, where H increases at the same location as δ^*, and reaches a maximum at the location where θ begins to increase. This well-defined H peak aligns with the experimental results [22], with the exception of the upstream shift in LSB reattachment location that was also identified in the 7° AOA C_p results (Fig. 5). In the 1° AOA result, the values from $x/c = 0.9$ to the TE are elevated, which is attributed to the unsteady nature of the separated suction side BL interacting with the pressure side BL. This difference is only seen in the 1° AOA result, since the $5^\circ$and 7° AOAs have a more stable turbulent BL at the TE.

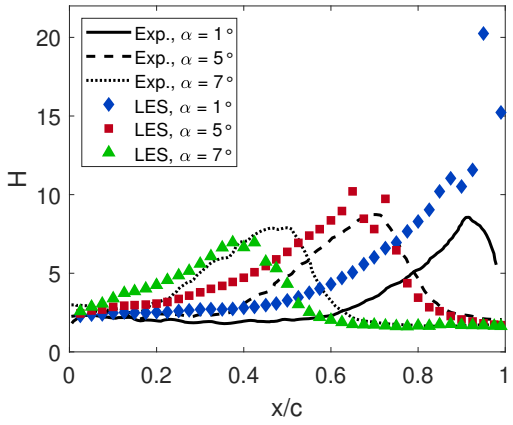

Fig. 8. Suction side H for $\alpha = 1^\circ, 5^\circ, 7^\circ$, compared with experimental measurements [22]

Shape factor, H, results provide a very clear location of BL transition (summarized in Table 2), which is difficult to resolve using either the C_p plots or through visualization methods. This H behaviour is not commonly included in the analysis of low Re airfoil simulations, however the LES results of Lobo *et al.* [19], the experimental measurements by McAuliffe and Yaras [35] and the simulated flat plate results by Lardeau *et al.* [11] and Wissink and Rodi [5] captured a similar H pattern, with peak H values in the range of 6 to 12. Additionally, while Ziade *et al.* does not present H as a function of x/c for their simulated airfoil, H was found to range from 5.9 in the attached BL up to a peak value of 22 [16]. The simulated H values for each AOA fall within the

range found for other transitional separated BLs, with peak values of 11, 10.2, and 7.0, and more importantly these values are in agreement with the experimental data available for the SD 7037 airfoil [22]. This indicates that the LES simulation captured the correct velocity distribution and BL profile shape compared to the experimental results, validating the accuracy of the mean velocity behaviour through the complex flow behaviour in the transitional separated BL.

As the BL completes the transition to turbulence, θ increases in relation to δ^* and causes H to decrease to a magnitude lower than the value in the laminar BL. For a flat plate BL with no pressure gradient, the typical H values are approximately 2.4 for a laminar BL and 1.7 for a turbulent BL [5]. In agreement with these values, the laminar BL at the LE of the airfoil for all simulated AOAs has H ranging between 2.3 to 2.6, and 5° and 7° AOA have H values of 1.7 and 1.6 in the turbulent BL at the TE of the airfoil. Additionally, the location where H values begin to plateau at the turbulent BL value of 1.7 aligns with the simulated reattachment location predicted from the end of the transition ramp in the C_p plots. The analysis of the transitional separated BL using H has excellent agreement with the experimental data, and strongly validates the LES prediction of the complex BL transition behaviour occurring in the separated BL.

Laminar Separation Bubble Visualization

With the location of the LSB more clearly defined using H, Fig. 9 shows a close-up view of the transient behaviour in the LSB for each AOA. These images are from the same timestep as the Q-criterion images in Fig. 4, and feature one set of pathlines that begins at the LE and a second set beginning within the LSB. For context, a contour of the non-dimensional velocity at the midplane of the airfoil span shows the low velocity within the LSB and the increase in velocity in the separated BL. All of the pathline scenes are on the same scale, which highlights the decrease in LSB thickness as the AOA increases.

For 1° AOA, the pathlines show laminar separation occurring at approximately $x/c = 0.55$, and multiple recirculation vortices within the LSB. These clockwise recirculation vortices are formed within the LSB due to the shear caused by the separated boundary layer [33], as shown in Fig. 1. Analysis by Roberts and Yaras [12] similarly identified multiple clockwise vortices, with local BL reattachment between them. This local reattachment can be seen clearly in the 1° AOA results

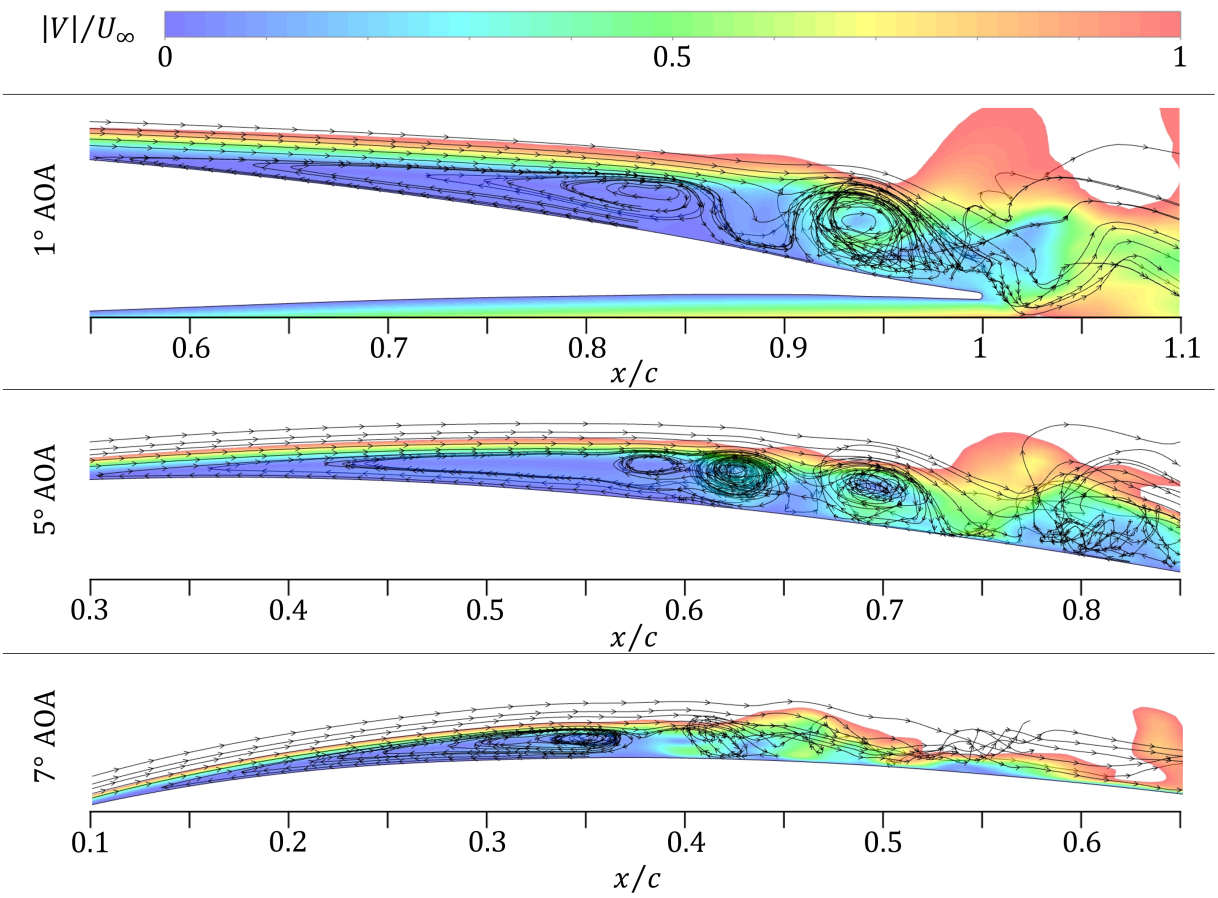

Fig. 9. Contours of $|V|/U_\infty$ vs. x/c for $\alpha = 1°, 5°, 7°$ with pathlines to visualize LSB. Image scale is consistent, with different x/c ranges

when pathlines are pulled from the separated BL down to the surface by one vortex (at $x/c = 0.875$), only to be pulled back up to the separated BL by the following vortex (at $x/c = 0.9$). Even though there is local transient reattachment, the separated boundary layer does not fully reattach to the suction side of the airfoil. From experiments [22], it is known that the suction side has a fully reattached BL at $3°$ AOA, and that trends in the location of the LSB indicate the separated shear layer is very near reattachment at the TE of the $1°$ AOA case. The pathlines do give the impression of a fully formed LSB due to the deviation of the suction side streamlines in the airfoil wake, caused by the interaction between the suction and pressure side BLs.

The $5°$ AOA pathline scene extends from $x/c = 0.3$ to 0.85, which is the length of the LSB as predicted by the time-averaged C_p and H. At the timestep selected for the image, the BL does

not fully reattach until $x/c = 0.9$ due to a pocket of low velocity which contains some reverse flow centred around $x/c = 0.8$. This low velocity region corresponds to the final spanwise roll and horseshoe structures, which can be seen in the Q-criterion results in Fig. 4 as the final dark red spanwise region before the TE. Additionally, the location of each vortex within the LSB (from $x/c = 0.55$ to 0.75) aligns with the x/c location of the K-H rolls in the separated BL visualized using Q-criterion (Fig. 4). The downstream progression of the K-H rolls and associated vortices leads to instantaneous pockets of low velocity and BL separation after the time-averaged BL reattachment location. This poses a challenge when defining the location of BL reattachment, since the time-averaged LSB does not provide a good representation of the transient behaviour occurring in the back half of the LSB.

A similar trend is seen in the 7° AOA pathlines, where the BL appears on the verge of reattachment from $x/c = 0.45$ to 0.6. This appears to be in disagreement with the quick development of complex flow structures visualized in Fig. 4, since it would be expected that this would result in a shorter LSB that reattaches earlier than the other simulated AOAs. However, it has instead resulted in a very thin and elongated LSB that is more disorderly when nearing reattachment. It is clear that while the BL transition appears to occur faster at 7° AOA than for the other simulated AOAs, it is not sufficient to cause earlier BL reattachment.

BL Separation and Reattachment

The location of BL separation and reattachment is difficult to identify using the previous results, since C_p and H indicate the start and end of the LSB through gradual slope changes and visualization using Q-criterion or pathlines are dependent on the time step selected. The skin friction coefficient, C_f, in the streamwise direction provides a time-averaged location of BL separation and reattachment because an attached BL has positive C_f and regions of BL separation will have $C_f \leq 0$. The simulated C_f is calculated using the time-averaged x-direction wall shear stress, and due to the airfoil curvature this is an approximation of the streamwise wall shear stress. The LSB for the simulated AOAs are located in regions of lower curvature where the error using the x-direction wall shear stress is minimal.

The 5° and 7° AOA cases clearly demonstrate the expected C_f behaviour, shown in Figs.

10(b) and 11(b), due to their fully formed LSBs. The LSB height, h, is plotted in Figs. 10(a) and 11(a) to visualize the LSB shape associated with the presented C_f behaviour, where h is defined as the location of zero time-averaged s-velocity (velocity tangent to the airfoil surface). After separation, C_f plateaus at a negative value and begins to decrease at a x/c location just before the BL transition location identified by the H peak (x/c of 0.65 for 5° AOA and 0.4 for 7° AOA). After the BL transition, there is a negative peak with a steep recovery to a positive C_f to indicate BL reattachment. This stronger region of reverse flow (negative C_f) at the airfoil surface can be attributed to growth of the clockwise vortices in the latter portion of the LSB, as seen in Fig. 9. The locations of BL separation and reattachment determined using C_f for all simulated AOAs are summarized in Table 2.

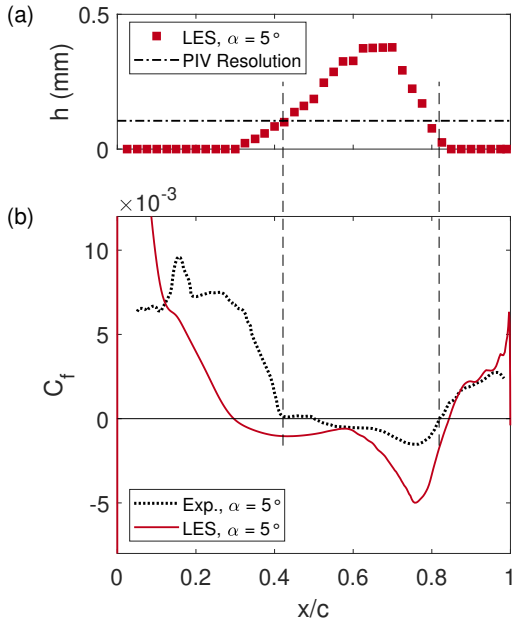

Fig. 10. $\alpha = 5^\circ$ (a) LSB height, h, compared with PIV resolution (b) Suction side C_f compared with experimental measurements [22]. Vertical lines indicate experimental BL separation and reattachment

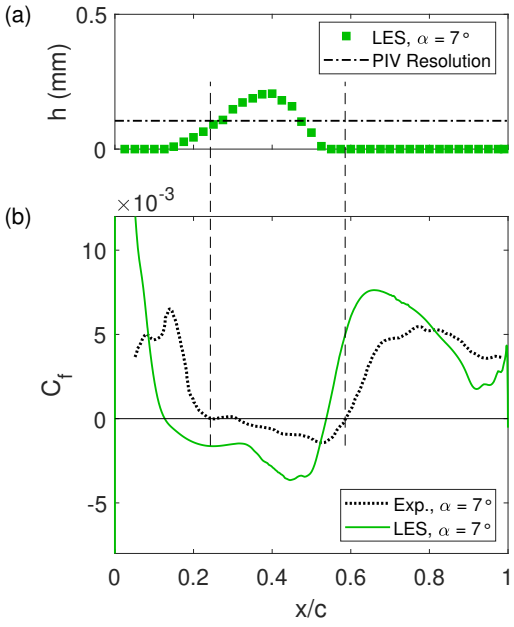

Fig. 11. $\alpha = 7^\circ$ (a) LSB height, h, compared with PIV resolution (b) Suction side C_f compared with experimental measurements [22]. Vertical lines indicate experimental BL separation and reattachment

These C_f trends are similar to previous LES and DNS works for transitional separated flow over cambered airfoils [2, 17–19], symmetric NACA airfoils [7, 8], a compressor cascade [11] and flat

plate geometries [11, 13]. As with the C_p results for this type of flow, the results in the referenced works are either unvalidated or validated against DNS results due to the lack of reliable experimental C_f data. Therefore the PIV post-processing technique used by Ghorbanishohrat [22] to experimentally determine C_f provides a unique opportunity to validate the BL wall shear behaviour predicted using LES.

The LES results predicted early BL separation in comparison to the experimental results for all simulated AOAs, though only the results for 5° and 7° are presented here. This is in contrast to the agreement in BL separation location found using C_p (Fig. 5), where experimental results were calculated using the same PIV data. This difference can be attributed to the PIV resolution at the airfoil surface, since the C_f accuracy is dependent on the measured velocity gradient close to the wall, whereas the C_p was calculated through integration of the entire velocity profile [22]. The PIV resolution of 0.105 mm is plotted against the LSB h in Figs. 10(a) and 11(a), showing that the near-wall mesh resolution in the LES simulation determines the velocity gradient closer to the wall than the PIV data. Due to this difference in near-wall resolution, any simulated h below the PIV resolution line would be experimentally measured as an attached BL, and therefore generate a positive C_f.

The vertical dashed lines on Figs. 10 and 11 are aligned with the experimentally predicted BL separation and reattachment locations, which are then compared against the LSB h. The experimental separation location is the same x/c location as the intersection between the simulated LSB h and the PIV resolution. This means that if the LES simulation had the same near-wall resolution as the PIV experiments, or vice versa, then the BL separation prediction would be in complete agreement. In terms of BL reattachment, the 5° AOA location is in agreement when factoring in the PIV resolution and the 7° AOA location has a similar upstream shift in reattachment to what was found in the C_p and H results. This shows that the difference in BL separation and reattachment locations in the C_f data is due to the differences in near-wall resolution only, validating the LES results for the highly transient and sensitive transitional separated BL on a cambered low Re airfoil.

CONCLUSION

A low Re cambered airfoil was simulated using wall-resolved LES to evaluate the ability of the simulation to predict the transitional separated BL, which includes a LSB. The simulations were performed using the SD 7037 airfoil, which is designed specifically for use in low Re applications, at the modest Re of 4.1×10^4 and AOAs of 1°, 5°, and 7°. Previous DNS and LES simulations of a transitional separated BL focused on flat plates, symmetric airfoils or compressor cascades, which differ in geometry from a modern cambered airfoil typically used in low Re applications. High quality experimental data on cambered airfoils at modest Re is very limited, and the results were validated against a particulary unique set of experimental data which included C_f. The range of AOAs selected for LES simulation covered a range of LSB locations, and the simulated behaviours of the transitional separated BL were validated at these different AOAs using multiple methods of comparison.

The qualitative analysis of the Q-criterion showed the expected behaviour of a transitional separated BL, including the formation of K-H rolls over the LSB which then broke down into large horseshoe vortices at BL reattachment. These horseshoe vortices were found to be on a larger scale with respect to the LSB length and size of the K-H rolls, when compared to higher Re simulations of symmetric NACA profiles. Additional visualization of the LSB using pathlines showed the transient nature of the BL reattachment, with large clockwise vortices within the LSB at the same instantaneous location as the K-H rolls. Within the LSB, these vortices created regions of local BL reattachment between them, and were found to continue into the reattached BL and created pockets of transient BL separation past the time-averaged location of reattachment.

The LES predicted suction side C_p results were of higher magnitude than the experimental data, however this was attributed to the near-wall PIV resolution and potential error introduced by the integration method used to calculate the experimental C_p. Of greater importance was the agreement of the C_p gradient with x/c, and the location of the transition ramp that is used to identify the LSB location on the airfoil surface. The location of the pressure recovery in the transition ramp for the 5°, and 7° AOA predicted a shorter LSB than was found experimentally, pointing to the possibility of a slight over-production of inflow turbulence using the built-in inlet turbulence model.

This however had no impact on the accuracy of the prediction of the BL separation location, and agrees with findings from a simulation with known under-production of free stream turbulence [16].

Analysis of the integral boundary layer properties was conducted to determine the locations of boundary layer separation, transition and reattachment. The δ^* and θ were compared to experimental data individually and then combined together to analyze trends in the shape factor, H. There was strong agreement with experimental data for the trends of all three parameters, with the exception of the early BL reattachment for 7° AOA. The values of H for the laminar and turbulent portions of the BL were aligned with expected flat plate values, and the peak H value used to indicate BL transition was a similar magnitude to previous works simulating a transitional separated BL.

Lastly, a comparison of simulated C_f with the unique low Re airfoil experimental data showed discrepancies in the locations of BL separation and reattachment, with PIV data predicting a shorter LSB. Through analysis of the simulated LSB height, this was determined to be caused solely by the difference in near-wall resolution between the LES and PIV data. The agreement of the C_f predicted separation and reattachment locations was a useful finding since the C_f predictions of the simulation provide a quick and accurate method of determining the precise LSB location on the suction side of the airfoil.

The presented analysis thoroughly validated the wall-resolved LES simulation of the transitional separated BL on the cambered SD 7037 airfoil through the pressure behaviour, velocity profiles, and the locations of BL separation, transition and reattachment. The modest Re case chosen for these simulations posed a computational challenge for many reasons, including the elongated chordwise region of natural BL transition and separated shear layer, when compared to previous computational works. This study has clearly shown the ability of LES to accurately capture the complex transient behaviour involved in the transitional separated flow over a low Re cambered airfoil.

ACKNOWLEDGEMENTS

The authors would like to acknowledge support from the Natural Sciences and Engineering Research Council of Canada (NSERC) and the use of the Digital Research Alliance of Canada resources. Funding from the Alexander Graham Bell Canada Graduate Scholarship-Doctoral (CGS-D) and the Ontario Graduate Scholarship (OGS) provided to Alison Zilstra helped support this research. The authors would also like to acknowledge the dedicated effort by Faegheh Ghorbanishohrat to produce high quality PIV data used for validation of these results.

REFERENCES

[1] Tani, I., 1964. "Low-speed flows involving bubble separations". *Progress in Aerospace Sciences,* **5**(C), pp. 70–103.

[2] Yuan, W., Khalid, M., Windte, J., Scholz, U., and Radespiel, R., 2005. "An investigation of Low-Reynolds-number flows past airfoils". *Collection of Technical Papers - AIAA Applied Aerodynamics Conference,* **1**(April 2015), pp. 102–120.

[3] Schlichting, H., and Gersten, K., 2017. *Boundary-Layer Theory*, 9th ed. Springer-Verlag Berlin Heidelberg.

[4] Hu, H., and Yang, Z., 2008. "An Experimental Study of the Laminar Flow Separation on a Low-Reynolds-Number Airfoil". *Journal of Fluids Engineering,* **130**(5), pp. 1–11.

[5] Wissink, J. G., and Rodi, W., 2006. "Direct Numerical Simulations of Transitional Flow in Turbomachinery". *Journal of Turbomachinery,* **128**(4), pp. 668–678.

[6] Brinkerhoff, J. R., and Yaras, M. I., 2011. "Interaction of viscous and inviscid instability modes in separation-bubble transition". *Physics of Fluids,* **23**(12).

[7] Thomareis, N., and Papadakis, G., 2017. "Effect of trailing edge shape on the separated flow characteristics around an airfoil at low Reynolds number: A numerical study". *Physics of Fluids,* **29**(1).

[8] Jones, L. E., Sandberg, R. D., and Sandham, N. D., 2008. "Direct numerical simulations of forced and unforced separation bubbles on an airfoil at incidence". *Journal of Fluid Mechanics,* **602**, pp. 175–207.

[9] Jones, L. E., and Sandberg, R. D., 2011. "Numerical analysis of tonal airfoil self-noise and acoustic feedback-loops". *Journal of Sound and Vibration,* **330**(25), pp. 6137–6152.

[10] Hoarau, Y., Braza, M., Ventikos, Y., and Faghani, D., 2006. "First stages of the transition to turbulence and control in the incompressible detached flow around a NACA0012 wing". *International Journal of Heat and Fluid Flow,* **27**(5), pp. 878–886.

[11] Lardeau, S., Leschziner, M., and Zaki, T., 2012. "Large Eddy Simulation of Transitional Separated Flow over a Flat Plate and a Compressor Blade". *Flow, Turbulence and Combustion,* **88**(1-2), pp. 19–44.

[12] Roberts, S. K., and Yaras, M. I., 2006. "Large-Eddy Simulation of Transition in a Separation Bubble". *Journal of Fluids Engineering,* **128**(2), pp. 232–238.

[13] Li, H. J., and Yang, Z., 2019. "Separated boundary layer transition under pressure gradient in the presence of free-stream turbulence". *Physics of Fluids,* **31**(10), p. 104106.

[14] Smith, T. A., and Ventikos, Y., 2019. "Boundary layer transition over a foil using direct numerical simulation and large eddy simulation". *Physics of Fluids,* **31**(12), p. 124102.

[15] Kim, H.-J., Lee, S., and Fujisawa, N., 2006. "Computation of unsteady flow and aerodynamic noise of NACA0018 airfoil using large-eddy simulation". *International Journal of Heat and Fluid Flow,* **27**(2), pp. 229–242.

[16] Ziadé, P., Feero, M. A., Lavoie, P., and Sullivan, P. E., 2018. "Shear Layer Development, Separation, and Stability Over a Low-Reynolds Number Airfoil". *Journal of Fluids Engineering,* **140**(7), pp. 1–12.

[17] Galbraith, M. C., and Visbal, M. R., 2008. "Implicit large eddy simulation of low-Reynolds-number transitional flow past the SD7003 airfoil". *46th AIAA Aerospace Sciences Meeting and Exhibit*.

[18] Breuer, M., 2018. "Effect of Inflow Turbulence on an Airfoil Flow with Laminar Separation Bubble: An LES Study". *Flow, Turbulence and Combustion,* **101**(2), pp. 433–456.

[19] Lobo, B. A., Schaffarczyk, A. P., and Breuer, M., 2022. "Investigation into boundary layer transition using wall-resolved large-eddy simulations and modeled inflow turbulence". *Wind Energy Science,* **7**(3), pp. 967–990.

[20] Islam, M., Langfeldt, F., Furst, J., and Wood, D. H., 2017. "CFD Analysis of a SD 7003 Airfoil with a Local Correlation Based Transition and Turbulence Model". *IOP Conference Series: Materials Science and Engineering,* **184**(1), pp. 1–6.

[21] Bartl, J., Sagmo, K. F., Bracchi, T., and Sætran, L., 2019. "Performance of the NREL S826 airfoil at low to moderate Reynolds numbers—A reference experiment for CFD models". *European Journal of Mechanics, B/Fluids,* **75**, pp. 180–192.

[22] Ghorbanishohrat, F., 2019. "Study of a low Re airfoil considering laminar separation bubbles in static and pitching motion". PhD thesis, University of Waterloo.

[23] Burgmann, S., Dannemann, J., and Schröder, W., 2008. "Time-resolved and volumetric PIV measurements of a transitional separation bubble on an SD7003 airfoil". *Experiments in Fluids,* **44**(4), pp. 609–622.

[24] SHARCNET, 2022. Digital Research Alliance of Canada.

[25] Gharali, K., 2013. "Pitching airfoil study and freestream effects for wind turbine applications". PhD thesis, University of Waterloo.

[26] Selig, M. S., Lyon, C. A., Giguere, P., Ninham, C. P., and Guglielmo, J., 1996. *Summary of low-speed airfoil data, Vol. 2*. SoarTech Publications, VA.

[27] Versteeg, H., Malalasekera, W., Orsi, G., Ferziger, J. H., Date, A. W., and Anderson, J. D., 1995. *An Introduction to Computational Fluid Dynamics - The Finite Volume Method*, 2nd ed. Pearson Education Limited, Harlow.

[28] Dhamankar, N. S., Blaisdell, G. A., and Lyrintzis, A. S., 2018. "Overview of turbulent inflow boundary conditions for large-eddy simulations". *AIAA Journal,* **56**(4), pp. 1317–1334.

[29] Orlando, S. M., 2011. "Laser Doppler Anemometry and Acoustic Measurements of an S822 Airfoil at Low Reynolds Numbers". Master's thesis, University of Waterloo.

[30] Pope, S. B., 2000. *Turbulent Flows*. Cambridge University Press.

[31] ANSYS Academic Research, Release 20.2. "ANSYS Fluent Theory Guide". In *ANSYS Help System*, 20th ed. ANSYS Inc.

[32] Hunt, J. C. R., Wray, a. a., and Moin, P., 1988. "Eddies, streams, and convergence zones in turbulent flows". In Proceedings of the Summer Program, no. CTR-S88, Center for Turbulence

Research, pp. 193–208.

[33] Russell, J. M., 1979. *Length and Bursting of Separation Bubbles: A Physical Interpretation*. NASA. Langley Res. Center The Sci. and Technol. of Low Speed and Motorless Flight, Pt. 1.

[34] Lang, M., Rist, U., and Wagner, S., 2004. “Investigations on controlled transition development in a laminar separation bubble by means of LDA and PIV”. *Experiments in Fluids,* **36**(1), pp. 43–52.

[35] McAuliffe, B. R., and Yaras, M. I., 2005. “Separation-Bubble-Transition Measurements on a Low-Re Airfoil Using Particle Image Velocimetry”. In Volume 3: Turbo Expo 2005, Parts A and B, Vol. 3 PART B, ASMEDC, pp. 1029–1038.